Structural Engineering and Mechanics, *Vol. 74, No. 2 (2020) 201-214*
DOI: https://doi.org/10.12989/sem.2020.74.2.201

Performance evaluation of composite moment-frame structures with seismic damage mitigation systems using wavelet analyses

Mosbeh R.Kaloop[1,2,3a], Hong Min Son[1,2b], Hyoung-Bo Sim[1c], Dongwook Kim[1d] and Jong Wan Hu*[1,2]

[1]*Department of Civil and Environmental Engineering, Incheon National University, Incheon 22012, Korea*
[2]*Incheon Disaster Prevention Research Center, Incheon National University, Incheon 22012, Korea*
[3]*Public Works and Civil Engineering Department, Mansoura University, Mansoura 35516, Egypt*

(Received March 28, 2019, Revised November 4, 2019, Accepted November 21, 2019)

Abstract. This study aims at evaluating composite moment frame structures (CFS) using wavelet analysis of the displacement behavior of these structures. Five seismic damage mitigation systems' models of 9-story CFS are examined namely, basic (Model 1), reinforced (Model 2), buckling restrained braced (BRB) (Model 3), lead rubber bearing (LRB) (Model 4), and composite (Model 5) moment frames. A novel integration between continuous and discrete wavelet transforms is designed to estimate the wavelet power energy and variance of measurements' behaviors. The behaviors of the designed models are evaluated under influence of four seismic loads to study the dynamic performance of CFS in the frequency domain. The results show the behaviors of models 3 and 5 are lower than other models in terms of displacement and frequency performances. Model 3 has been shown lower performances in terms of energy and variance wavelets along the monitoring time; therefore, Model 3 demonstrates superior performance and low probability of failure under seismic loads. Furthermore, the wavelet variance analysis is shown a powerful tool that can be used to assess the CFS under seismic hazards.

Keywords: composite frame; wavelet; dynamic analysis; seismic

1. Introduction

Nowadays, the composite moment resisting frames structures (CFS) with control systems have been widely used in constructions to reduce disaster impacts that occurred during sudden effect, such as seismic loads (Mehanny and Deierlein, 2000, Hu *et al.* 2010, Rhee *et al.* 2012, Hu and Choi, 2014, Min, 2017). The CFS systems are efficient in terms of the used materials and eliminating field welding of beam-column connections; moreover, it can be also used in high seismic regions (Mehanny and Deierlein, 2000, Farrokhi *et al*. 2010, Shi *et al.* 2018, Shallan *et al*. 2018). The main parts of CFS frames are the columns and connections between structures' members. The advantages of concrete-filled steel tube (CFT) columns greatly outweigh the advantages of composite steel-concrete columns and suite for moment-resisting frames in high seismic zones (Hu *et al.* 2010, Hu and Choi, 2014). The current study uses CFT composite columns and steel beams and that were modelled as nonlinear beam-column elements to conduct the CFS system. Two-dimension discrete fibre sections placed in the integration points of nonlinear beam-column elements are used to simulate the cross-section of CFT columns and steel beams as presented in (Hu *et al.* 2010, Min, 2017).

Herein, although the performances of deformation capacity of CFS systems are evaluated and studied previously (Hu, 2008, Park *et al.* 2011, Min, 2017, Lee *et al.* 2018, Matarazzo *et al.* 2018, Shi *et al.* 2018), the research on the behavior of buildings with different kind of control systems seems not deeply investigated enough at this moment, particularly in frequency domain. In addition, the time series of wavelet power evaluation of frames behaviors is not used and discussed in detail for the CFS systems. Meanwhile, many methods were used to evaluate the performance of CFS sections, members and connections, under different seismic loads (Park *et al.* 2011, Min, 2017). Mehanny and Deierlein (2000, 2001) evaluated the damage of six-story frame using statistical analysis, a damage index method, in the time domain, and they applied seismic loads to study the frame performance. It was found that the nonlinear behavior can be estimated using the damage index, but other performance levels should be accurately evaluated. Also, Matarazzo *et al*. (2018) utilized the damage index to evaluate damage cases of CFS. Shi *et al*. (2018) tested a full-scale CFS, which is steel frame composed of box cold-framed columns, hot-rolled I-section beams, end-plate joints, flexible braces, and stud-connected prefabricated slabs, under cyclic loads. They used statistics evaluation in the time domain to assess the deformations and base shear performances; in addition, they evaluated the

*Corresponding author, Associate Professor
E-mail: jongp24@inu.ac.kr
[a] Associate Professor
E-mail: mosbeh@mans.edu.eg
[b] Researcher
E-mail: bluekaris@nate.com
[c] Professor
E-mail: hbsim@inu.ac.kr
[d] Associate Professor
E-mail: dwkim@inu.ac.kr

ISSN: 1225-4568 (Print), 1598-6217 (Online)

energy dissipation performances of the model and found that it can be applied to assess the frame's behavior. Hu and Roberto (2011) assessed four and six stories of CFS in linear and nonlinear analyses using the statistical analysis in the time domain for the movements, applied loads, base shear coefficients and the rotation; a smart development connection was used in their study and evaluated. They found that the development connection performance was better in the time domain; this system is used in the current study. Park *et al*. (2011) assessed 3-, 9- and 20-stories of frames that designed using CFT, and they evaluated the performances of frames utilizing the statistical analysis of stress and strain of frames performances. From this literature, it can be seen that most researches applied statistical analyses in the time domains or traditional methods to evaluate the behavior of CFS systems.

This study investigates the use of wavelet variance and energy to evaluate different cases of CFS under seismic loads. Obviously, the wavelet analysis is widely used to evaluate the dynamic behavior of different applications of engineering, especially in evaluating the behavior of structures under dynamic loads (Taha, 2006, Chen and Gao, 2011, Kaloop and Hu, 2016). Chouinard *et al*. (2019) utilized wavelet analysis to detect the damage of beams, and their results showed that the wavelets are efficient into detecting and localizing low of damage. And the verification of used wavelet to identify damage of structures was assessed by using experimental and theoretical studies, and the results showed that the wavelet is effective to detect the damage (Li *et al*. 2018). Farzampour *et al*. (2018 a,b) evaluated the performance of controlled structures using integrated wavelet and independent component analysis, and they found that this method is sufficiently robust in an accurate extraction of dynamic modes. But the wavelet variance and energy were not used yet to assess the performance of CFS. To illustrate this point, Iliuk *et al*. (2014) used wavelet spectrum and time-frequency map to extract the dynamic characteristic of regular and irregular dynamic systems, and they concluded that the wavelet analysis can be used beside traditional tools to extract the dynamic behaviors of structures. The wavelet variance of the dynamic component of ground-water is extracted by Xing *et al*. (2018) to monitor the dynamic movement of groundwater level, and they found that the wavelet is suitable and reliable to study the groundwater dynamics. Furthermore, the wavelet has been applied to study the rate of the changes of temperature, and the results show the wavelet is an effective tool to extract that changes (Jemai *et al.* 2017). Meanwhile, the wavelet is one of the efficient methods that can be used to evaluate historical and development structures (Taha, 2006, Stefano *et al.* 2016). The wavelet energy was used to assess the dynamic behavior of bridges (Sayed *et al.* 2017) and buildings (Kaloop *et al.* 2016). The main advantage of wavelet analysis is the wavelet coefficients or scales which deduced from time-sequential measurement data represents the components of energy input in the time and frequency domains (Kaloop *et al.* 2016, Sayed *et al.* 2017). The decomposition energy can be used to distinguish between the frequencies contents and distributions of it with measurement time, so the wavelet power, energy, and variance of signal measurements can be estimated and presented (Chan, 1995). In other words, the time series of wavelet energy and variance allow representing the frequency change into monitoring time. More details for wavelet theory and assessment can be found in (Chan, 1995, Xiaoyan *et al.* 2000, Sun, 2002).

Five models, in the current study, are developed and assessed in the vibration and structures laboratory at Incheon National University (Min, 2017). The five models are presented in the following section. Min (2017) simulated the five models using OpenSees software and used statistical analysis to evaluate the performance of five models. The main difference between the five models is in the damage mitigation system or control system used in each model. This study extends Min's (2017) evaluation. Therefore, to complete the evaluation of five models in the frequency domain, a novel integration between wavelet transforms is implemented to assess the wavelet energy and variance of the behavior of these models. Four ground motions are considered to assess the behavior of five models and evaluate the results of time series of wavelet variance and energy performances. The roof's displacements of frames are extracted using a finite element model and evaluated in this study.

2. Models, Loads and Methods

2.1 Models design

In the current study, the models are designed and used to evaluate the performance of five kinds of control systems of CFS structures subjected to different ground motions. To simulate the behavior of real structures, three frames are connected in three dimensions (3D). The three frames A, B, and C are connected in a square plan, and that includes nine stories as presented in Figure 1. The dimensions of the frames are presented in Figure 1. Table 1 illustrates the sections of I-beams that used to simulate the beams of the building floor. The internal and external columns are composite sections, see Figure 1.b; it is a rectangular CFT, and the joint between columns and beams is presented in Hu *et al*. (2010) and Min (2017). The joint is designed as a moment connection as presented in Hu *et al*. (2010) and Min (2017). The five models, as can be seen in Figures 1 and 2 and Table 2, includes the three frames A, B, and C, and the models are considered as 2D half symmetric frame model because of their regular quadrilateral (Hu and Choi, 2014, Kim and Leon, 2007). Rigid links connectors are used to construct single multi-point constraint objects which are able to constrain the translational degree of freedoms between slave nodes allocated on the gravity frames (B and C) and master nodes allocated on the perimeter moment frame (A) (Hu and Choi, 2014). The columns' sections are presented in Figure 1.b; the model that designed by basic sections (CFT section) was named model 1 (basic model), a reinforcement section (RS) is added to model 1 with height 549 mm at ground floor and 396 mm at first and second floors for model 2 (reinforced model). The buckling

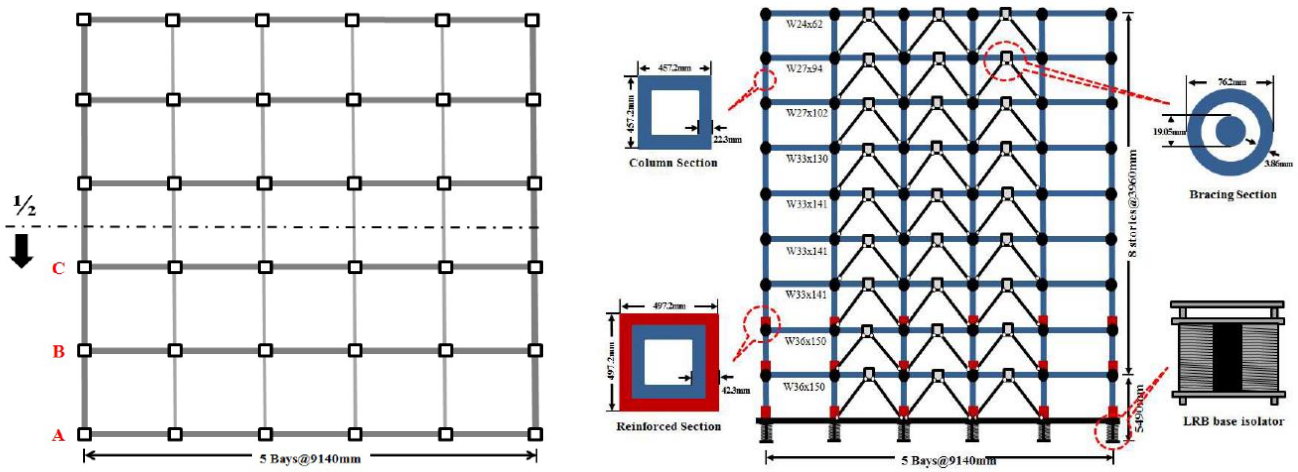

(a) (b)

Fig. 1 Model design system (a) plan and (b) view of model 5 components on frame A

Table 1 Specification of I-beams of floor beams (unit in inch)

Beam size	d	t_w	b_f	t_f
W24x62	23 ¾	7/16	7	9/16
W27x94	26 7/8	½	10	¾
W27x102	27 1/8	½	10	13/16
W33x130	33 1/8	9/16	10 ½	7/8
W33x141	33 ¼	5/8	10 ½	15/16
W36x150	35 7/8	5/8	12	15/16

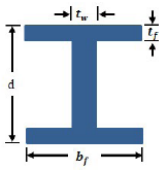

Table 2 Summary of five model components

model	components				Notice
	CFT	Including RS	Including BS	Including LRB	
1	O	X	X	X	Fiber section is used at ground floor
2	O	O	X	X	
3	O	X	O	X	
4	O	X	X	O	
5	O	O	O	O	

restrained braced (BRB) system is used in model 3 (BRB model) and lead-rubber bearing (LRB) base isolation system is used in model 4 (LRB model). All previous properties are emerged in model 5 (composite model), see Figure 2. Table 2 illustrates the difference between the five models, and Figure 2 presents Model 5. The OpenSees finite element (FE) program is used to simulate the five models. The five models are designed and developed by the vibration and structures laboratory at Incheon National University, South Korea, (Hu, 2008, 2015, Hu and Roberto, 2011, Seo and Hu, 2016, Mansouri, Amiri, *et al.* 2017, Mansouri, Hu, *et al.* 2017, Min, 2017, Mansouri *et al.* 2018), and the models are evaluated and assessed using statistical and traditional methods (Min 2017).

2.2 Considering loads

According to ASCE 7-05 and IBC2006 specifications, all frames represented a building located on a stiff soil site (Hu and Choi, 2014). The seismic design category (SDC) is considered to be a high seismicity area as specified for class D in the ASCE 7-05 (Hu and Choi, 2014). The other basic conditions used for building design are presented in Table 3; see Figure 2 for the dead and live loads (DL and LL) distributions. Meanwhile, to examine the effect of five model design and performance, four ground motions are selected to simulate seismic loads. The Lose Angeles (LA) and Seattle (SE) ground motions are selected and developed from both historical records and simulations as part of the FEMA/SAC project on steel moment frames (Hu and Roberto, 2011). 40 ground motions of LA and SE regions are evaluated and assessed in Min (2017). Here, LA14, LA28, SE04 and SE28 have been selected and used in the current study. The LA14 and SE04 ground motion were assumed to be subjected to a 10% probability of exceedance in 50 years (10% in 50 years), while LA28 and SE28 ground motions were assumed to be subjected to a 2% in 50 years, corresponding to the design-based earthquake (Min, 2017)

Figure 3 illustrates the acceleration measurements of the four ground motions. The peak ground acceleration (PGA) of LA14, LA28, SE04, and SE28 are 0.66, 1.33, 0.66, and 1.39 g respectively. The PGA is observed at 4.32, 4.20, 4.48, and 8.50 seconds for the ground motions LA14, LA28, SE04, and SE28, respectively. In addition, Figure 4 demonstrates the spectrum response of the ground motions. Furthermore, the scale of the average spectrum of LA 21-40 and design spectrum are presented in Figure 4.b. To solve the time-dependent dynamic problem, a transient equilibrium analysis was performed using the Newmark method (Hu 2008, Hu and Roberto 2011, Min 2017). A value of 2.5% was used for the damping as defined by the Rayleigh command in the OpenSEES program (Hu and Roberto 2011), and according to the current design guidelines for the composite frames (e.g ASCE7-05 and IBC2006). The conclusion of response spectral accelerations of forty ground motions of LA and SE earthquakes according to five models are presented in Table

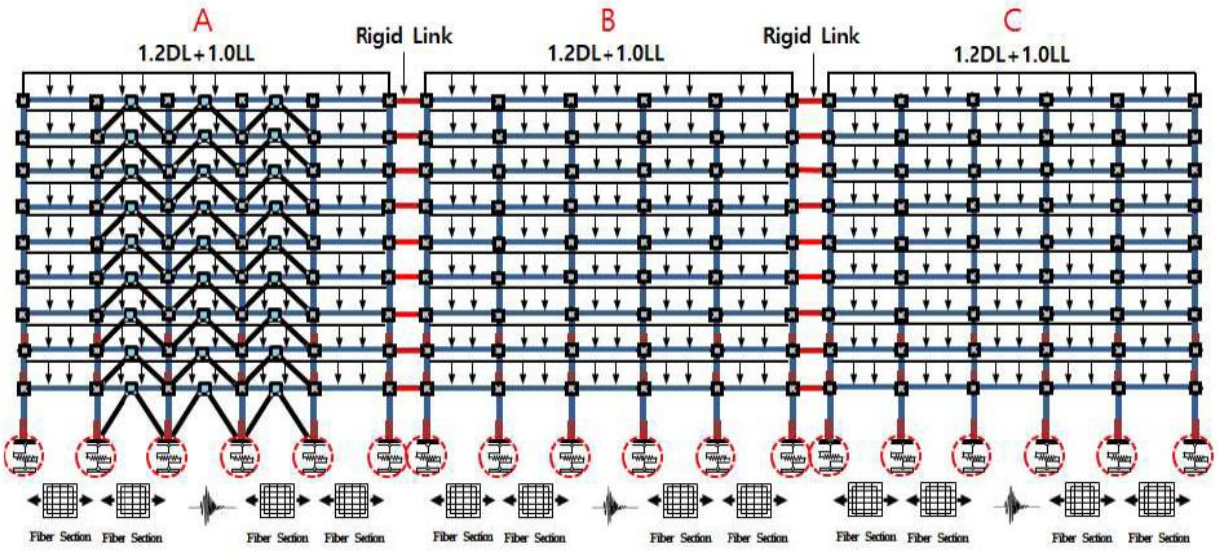

Fig. 2 Model 5 diagram

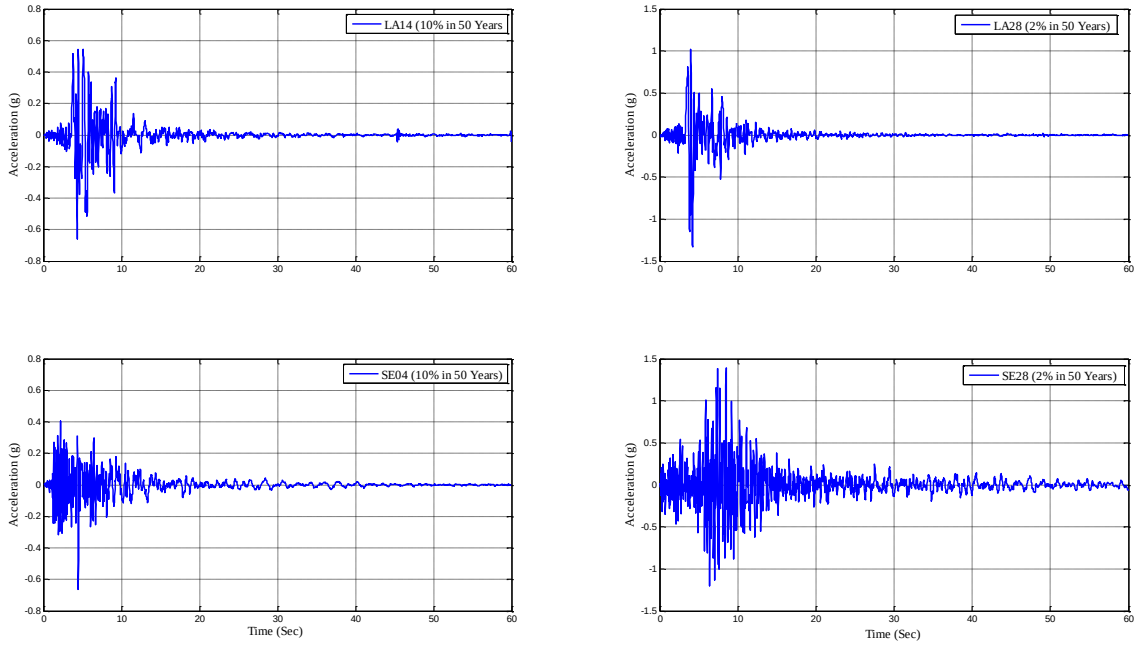

Fig. 3 Acceleration history over time for four earthquake accelerations

Table 3 Basic conditions for building design (Hu and Choi, 2014)

Located area	Loads (Other)	Loads (Roof)	SDC	Site condition	Occupancy category
LA area	DL: 4.12 kPa LL: 2.39 kPa	DL: 4.05 kPa LL: 0.96 kPa	D class	Stiff soil (class D)	Ordinary structure

4. The spectral acceleration was calculated using the design spectrum and scaled the average spectrum of ground motions for each subjected probability of exceedance in 50 years (2 and 10%). From Table 4, it can be seen that the dominant frequency of models is in between 0.617 to 0.85 Hz's.

Table 4 The average response acceleration (Sa) for the natural period and LA and SE earthquakes of each model

Model	T (Sec)	LA		SE		Design	
		Sa (g) – at 10%	Sa (g) – at 2%	Sa (g) – at 10%	Sa (g) – at 2%	Sa (g) – at 10%	Sa (g) – at 2%
1	1.52	0.40	0.70	0.37	0.60	0.39	0.58
2	1.30	0.51	0.79	0.49	0.68	0.45	0.68
3	1.17	0.54	0.79	0.61	0.82	0.50	0.75
4	1.62	0.36	0.67	0.34	0.57	0.36	0.54
5	1.49	0.41	0.71	0.38	0.60	0.39	0.59

In addition, from Table 4, the maximum spectral of LA and SE ground motions is 0.54, and 0.61 g, respectively, and that can be observed in model 3. Also, the design

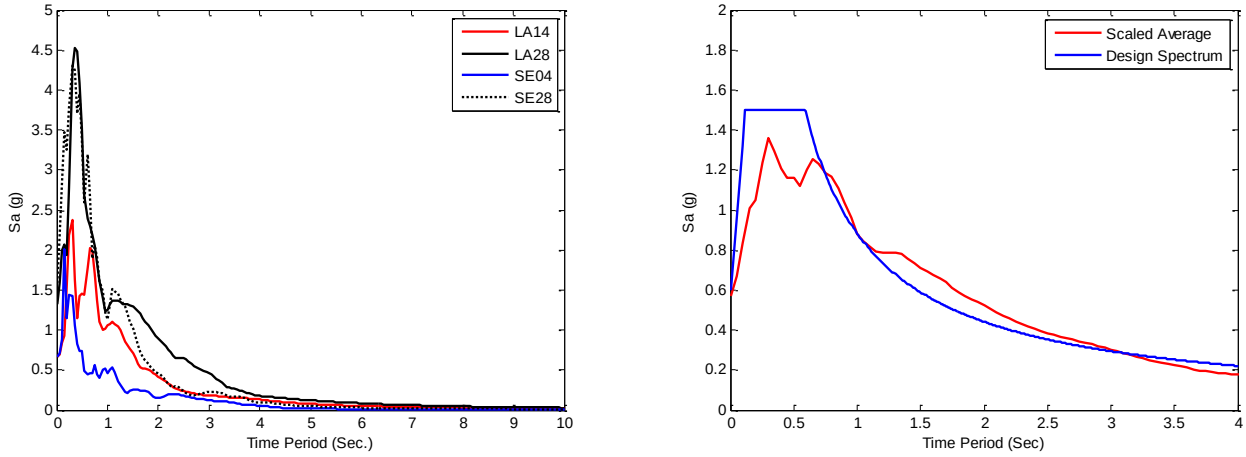

(a) (b)

Fig. 4 (a) Seismic response spectrums of selected ground motions, (b)average and design response of 2% in 50 years (LA 21-40)

spectrum of model 3 is shown higher than other models (0.50 and 0.75 g for 10 and 2% probability of exceedance, respectively).

2.3 Wavelet variance and energy

The wavelet is used to refer to either orthogonal, discrete wavelet transform (DWT), or nonorthogonal, continuous wavelet transform (CWT), wavelets (Torrence and Compo, 1998). The CWT is useful for time series analysis (Torrence and Compo, 1998); in addition, the DWT is more useful because the transformed data have no redundant component (M.A. Sayed *et al.* 2017). Therefore, both wavelet methods are used in this study. The DWT is used to estimate the wavelet decomposition of signals to estimate the smoothed signals, reconstructed data, and calculate the total wavelet energy, and the reconstruction signal is used in CWT to estimate the wavelet variance. More details for the DWT and CWT can be found in (Rioul and Vetterli, 1991, Chan, 1995, Kijewski and Kareem, 2003, Taha, 2006, Chen and Gao, 2011).

In this study, the wavelet decomposition and energy calculation are estimated by DWT. In DWT, the signal (x(t))is divided into approximate components (a(t)), low-pass frequency level, and detail component (d(t)), high-pass frequency level (Taha, 2006). The approximate component is a smoothed signal or semi-static component of the signal measurements, while the detail component refers to the dynamic component of the measurements (M.A. Sayed *et al.* 2017). Therefore, the decomposition of the original signal can be expressed as:

$$x_j(t) = a_{j+1}(t) + d_{j+1}(t) \quad (1)$$

where, j represents the level number of frequency content of the signal. The range of frequency (ω) of each decomposition level is denoted as:

$$\omega_j = [\omega_{1j}, \omega_{2j}], w_{1j} = \frac{1}{2^{j+1}\Delta t}, w_{2j} = \frac{1}{2^j \Delta t} \quad (2)$$

where, Δt is the time step of the collection data, in this study the sampling frequency of signals is 50 Hz. Therefore, Table 5 demonstrates the frequency and time ranges of seven decomposition levels that are selected based on dominant frequency of models, as presented in Tables 4 and 5. Herein, it should be mentioned that six decomposition levels are used only with models 2 and 3, since the optimum time interval of those models is observed at level six (Table 5).

After that the smoothed data can be reconstructed using the detail components without loss any significant information of the original signal:

$$x(t) = \sum_{j=1}^{N} d_j(t) \quad (3)$$

where, N is the number of decomposition levels; herein, the detail components can be expressed using the linear combination of the wavelet basis function as follows:

$$d_j = \sum_{-\infty}^{\infty} C_{j,k} \varphi_{j,k} \quad (4)$$

where, k is the time scale index, $C_{j,k}$ are the wavelet coefficients, and $\varphi_{j,k}$ are the basis wavelet functions, which can be represented as follows:

$$\varphi_{j,k} = 2^{j/k} \varphi(2^j t - k) \quad (5)$$

Meanwhile, the total energy can be calculated by sum the squares of reconstruction signals; the energy of each decomposition level can be calculated by sum the squares of each detail level and the total energy can be represented using the decomposition levels as follows:

$$E = \sum_{j=1}^{N} \sum_{t=0}^{t} {d_j}^2(t) \quad (6)$$

After that, the CWT is used to extract the time-series

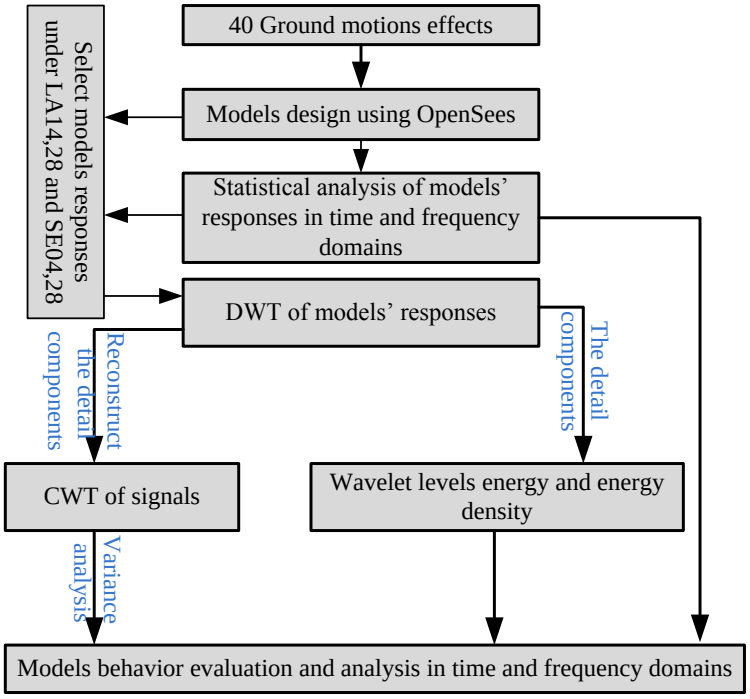

Fig. 5 Processing steps and evaluation of model's performances

Table 5 Frequency and time ranges of decomposition levels

Decomposition Level	Frequency Range (Hz)	Time Interval (Sec.)
1	25-50	0.02-0.04
2	12.5-25	0.04-0.08
3	6.25-12.5	0.08-0.16
4	3.125-6.25	0.16-0.32
5	1.562-3.125	0.32-0.64
6	0.781-1.562	0.64-1.28
7	0.781-0.391	1.28-2.56

variance of the reconstruction signals (x_n). The CWT of x_n is defined as the convolution of x_n with a scaled and translated version of the wavelet function:

$$W_n(s) = \sum_{m=1}^{M-1} x_m \varphi^*\left[\frac{(m-n)\Delta t}{s}\right] \quad (7)$$

where, the complex conjugate is denoted as (*), S is wavelet scale and n are the localized time index. M is the number of observations. To select the wavelet scale, an arbitrary set of scales can be used to build up a complete picture of wavelet power (Torrence and Compo, 1998). The appropriate scales can be extracted as follows:

$$S_j = S_0 2^{j\delta j} \quad j = 0,1,2,\ldots,J \quad (8)$$

$$J = \delta j^{-1} \log_2(M\Delta t/S_0) \quad (9)$$

where, S_0 is the smallest resolvable scale and J determines the largest scale. The S_0 should be chosen so that the equivalent Fourier period is approximately $2\Delta t$. The choice of a sufficiently small δj depends on the width in spectral-space of the wavelet function. For the Morlet function, it is about 0.5 (Torrence and Compo, 1998).

The average wavelet variance of reconstructed data is calculated using the CWT, which expressed by the equivalent of Parseval's theory as follows:

$$\sigma^2 = \frac{\Delta j \Delta t}{C_\Delta M} \sum_{n=0}^{M} \sum_{j=0}^{J} \frac{|W_n(s_j)|^2}{s_j} \quad (10)$$

where, C_Δ is scale independent, J is the largest scale and Δj is the width of spectral-space of the wavelet function. The Daubechies 6 (db6) and Morlet wavelet functions are used in DWT and CWT, respectively (Torrence and Compo, 1998, M.A. Sayed *et al.* 2017). Herein, the low total energy and variance of wavelet indicate that the structure is more stable and controlling. Here, Figure 5 illustrates the processing steps to evaluate the model's performances.

3. Results and discussions

The probability of the behavior of the five models behaviors is evaluated under forty ground motions of LA and SE areas in Min (2017). The roofs displacements, inter-story drift ratio displacement, connection rotation displacement, and base shear force were also examined. The results of the five models' performances show that the behavior of models 3 and 5 are almost the same. As previously mentioned, from Min (2017) focused on using statistical and traditional analyses in the time domain to assess the model's behaviors. Here, the displacements of the roof are used to assess the performances of the five models in the frequency domain which enables reaching more detailed information. Figure 6.a shows the displacements of models 3 and 5 under the ground motions LA 14, 28 and SE

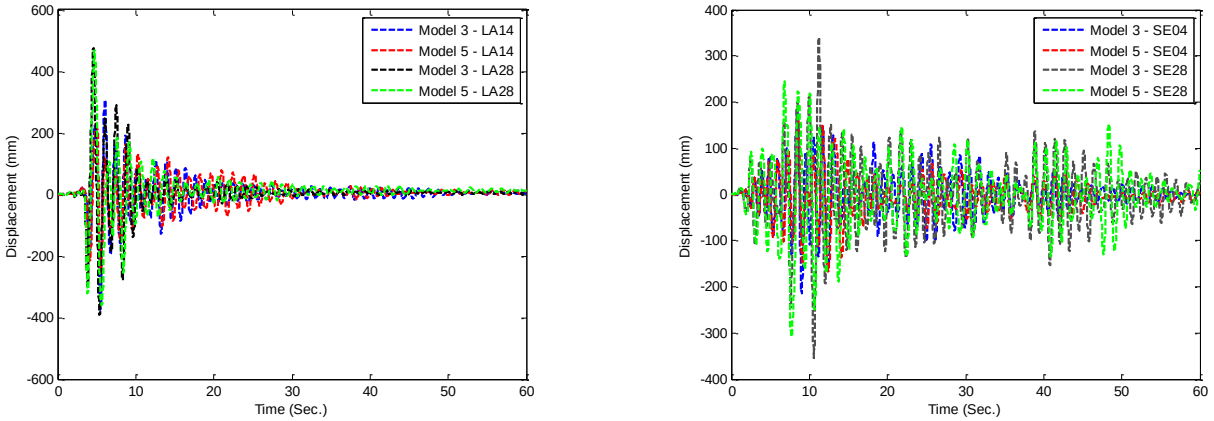

(a)

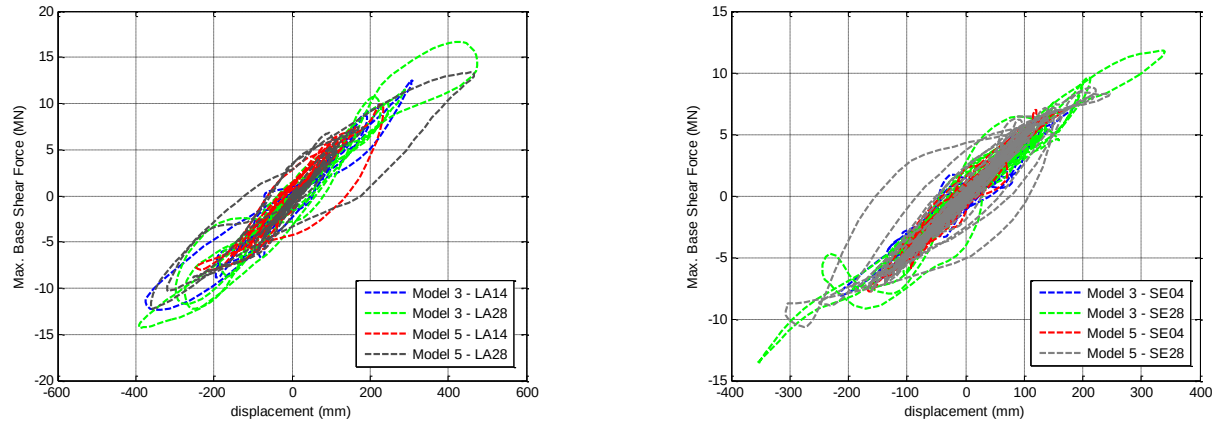

(b)

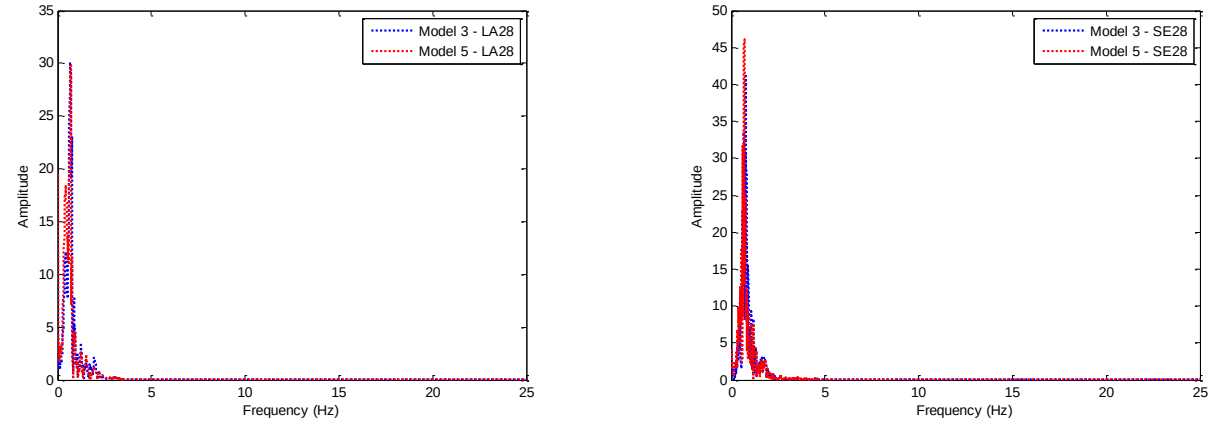

(c)

Fig. 6 Models 3 and 5 performances under seismic loads (a) time series displacement, (b) displacement-force curve, (c) frequency-amplitude curve

04, 28. In addition, Table 6 demonstrates the maximum displacement observed for the five models. From Figure 6.a and Table 6, it can be seen that the maximum displacement/movement (Desp.) occurred in models 2 and 1 under seismic LA14 and 28, respectively; while the maximum displacement is observed in model 2 under SE04 and SE28. Furthermore, the minimum displacement is recorded at model 5 under seismic loads LA14, LA28, and SE04. These results indicate that the performance of model 5 is better. But, obviously, the decline of displacement with time is shown, clearly, with model 3. In addition, minimum displacement is observed at model 4 under seismic load SE28. Therefore, to estimate the best model, we should study the behaviors of models under all ground motions as presented in Min (2017).

Figure 6.b presents the displacement and base shear

Table 6 Summary the model's behaviors

Models	LA14				LA28			
	Disp. (mm)	BSF (MN)	Frequency (Hz)	Amplitude (mm)	Disp. (mm)	BSF (MN)	Frequency (Hz)	Amplitude (mm)
1	-500.05	13.77	0.6473	72.16	656.45	-17.54	0.635	133.2
2	-530.96	14.15	0.6595	80.3	652.40	19.61	0.6473	136.4
3	-374.62	12.49	0.7938	32.82	475.54	16.69	0.6595	30.16
4	388.21	10.94	0.5496	30.8	598.97	13.91	0.6106	76.4
5	-245.62	9.93	0.7328	34.3	466.79	13.37	0.6961	29.83
	SE04				SE28			
1	-359.37	-11.76	0.6473	103.5	524.26	-16.34	0.6473	142.3
2	-364.49	-12.21	0.6473	88.35	610.16	-17.72	0.6473	146.7
3	-214.87	-8.09	0.8183	35.13	-354.71	-13.65	0.7938	41.13
4	321.26	-8.77	0.5862	46.46	289.18	-9.85	0.5984	121.7
5	171.38	-7.80	0.7084	18.8	-306.44	-10.64	0.6961	46.16

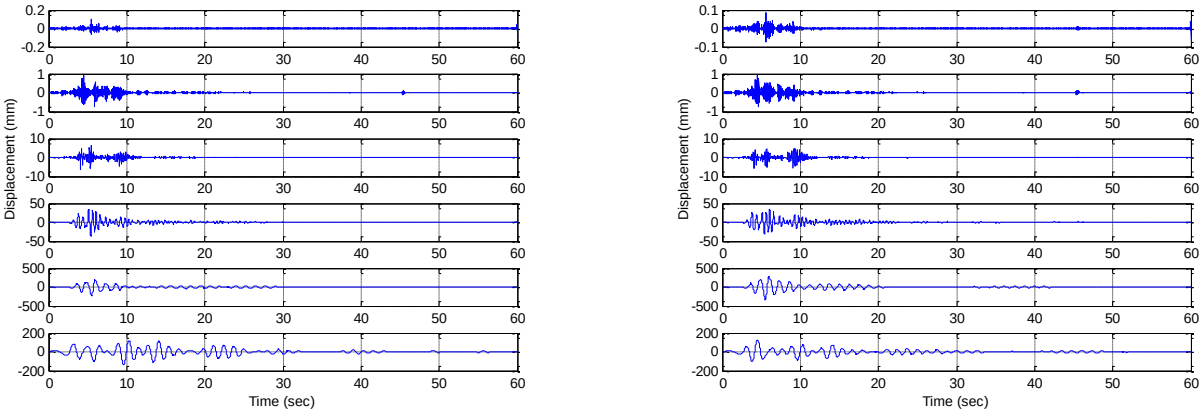

(a) Detail wavelet components with LA14 for model 5(left) and model 3 (right)

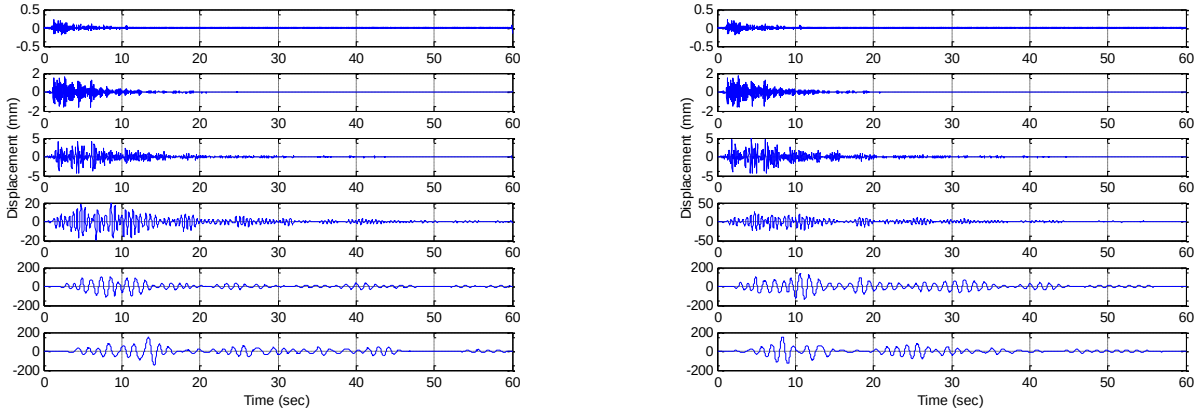

(b) Detail wavelet components with SE04 for model 5 (left) and model 3 (right)

Fig. 7 Detail wavelet components performances of models 3 and 5(the levels 1 to 6 from above to down)

force (BSF) relationship of models 3 and 5 under four seismic loads, and Table 6 illustrates the maximum BSF of five models under these loads. The BSF obtained for model 5 is smaller than other models except when the models subjected to SE28, it can be seen that the BSF of model 4 is lower. According to these findings, it could be concluded that model 5 has superior performance among the rest of the examined models. While the comparison of model 3 and 5 shows that the force-displacement curve is more sleepers with model 3. This reveals that the model 3 evidence

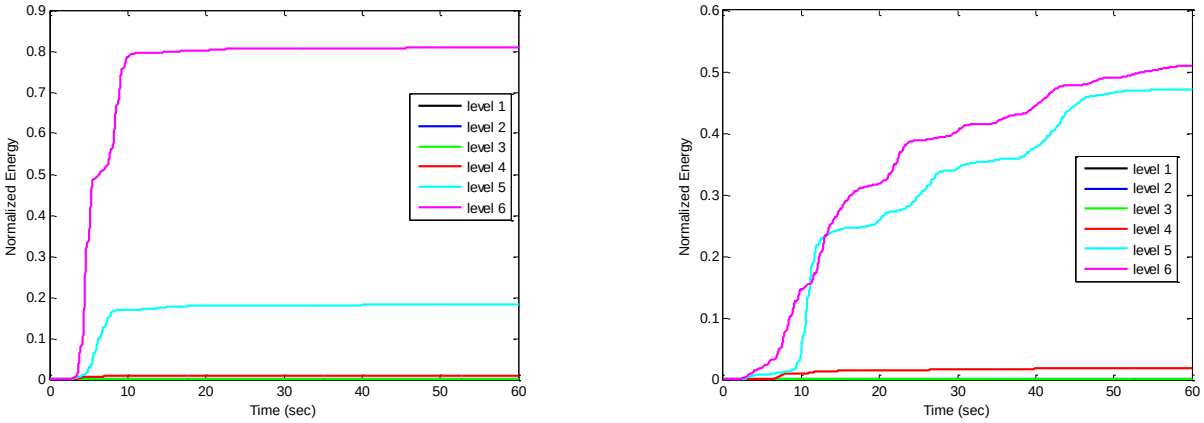

Fig. 8 wavelet energy of details reconstruction components of roofs' displacements of model 3 under (a) LA28 and (b) SE28 ground motions

shallower hardening after yielding, also, it is more permanent deformation during unloading.

In addition, Figure 6.c and Table 6 demonstrate the dominant frequency and maximum amplitude of the five models under the seismic loads. The minimum amplitude is obviously observed at models 3 and 5. In addition, the maximum frequency is observed in model 3. These imply that the performance model 3 has more stability in the frequency domain. From these results, it can be noticed that and the behavior of model 5 is better in the time domain, while in the frequency domain, the performance of model 3 is seemed better, as also it will be explained more in the following sections. Thus, the model's performances affect by the seismic characteristics in time and frequency domains and should be studied under all ground motions.

Consequently, the results of direct evaluation of the measurements are inadequate to estimate the real performance of the five models in the time domains, while the frequency domain is more credibly in assessing the performance of the examined structures. In addition, it can be noticed that the performance evaluation of models in the frequency domain is more clear in capturing the real behavior of the models. Herein, the wavelet is a reliable tool that can be used to represent the frequency response of signal in the monitoring time; wavelet energy and wavelet variance are suites to illustrate the powers of the measurements' frequencies over the monitoring time. Here, DWT is used first to remove the measurement noise and illustrate the energy of wavelet power at each wavelet levels. Figure 7 presents detail components of wavelet levels of models 3 and 5 under loads resulting from ground motions LA14 and SE04. The figure illustrates that the de-noise signals can be extracted using the wavelet analysis; it is clear that the wavelet levels five and six comprise the maximum displacements of frames' roofs. Furthermore, the noises contaminated the signals from wavelet' levels one to four. In addition, the maximum movements of roofs of models 3 and 5 are occurred at times 4.66 and 10.42 sec., respectively, with LA04. Similarity, the performance of two models under SE14 is almost the same, clear signals are shown at levels five and six, and the maximum displacements of models 3 and 5 are observed at 8.48 and 13.6 sec., respectively. These results reveal that the reaction of model 3 for absorbed sudden loads is high.

Furthermore, the energy of wavelet power at each wavelet levels are calculated and presented in Figure 8. Here, the detail components of signals are used only to rebuild the signals and calculate the energy of each detail reconstructed signals. The wavelet energy of model 3 performance under LA 28 and SE28 are implemented and presented in Figure 8.a and Figure 8.b, respectively. As it can be seen in Figure 8.a, the energy of level 6 is dominant, and arguably, it can be concluded that the high power of wavelet can be obtained from level 6 contents. However, level five still has some significant wavelet power, but it is clear that the power energy of other levels can be neglected. Meanwhile, the performance of model 3 under SE28, Figure 8.b, is seen different, the wavelet levels five and six are shown high significant, and arguably, the two levels possess almost same effectiveness to extract the model behavior in the time and frequency domains. Furthermore, the comparison between the performances of wavelet energy under two seismic loads imply the effectiveness of this method to evaluate the models behaviors; the energy of level six of model 3 under both seismic loads, LA28 and SE28, refer to the performance of model under SE28 is better than its performance under LA28, the energy of signals with SE28 is lower than that observed with LA28.

And the sharp change of wavelet energy is seen clearly under LA28. Therefore, the wavelet energy can be used to assess the behavior of models.

For that, the total and density of wavelet energy of five models are calculated and presented in Figures 9 and 10 under seismic LA28 and SE28. Figures 9.a and 9.b demonstrate the total energy of five models under LA28 and SE28, respectively. The cumulative energy with time is presented in the figures. From Figure 9.a, it can be seen that the total energy performance of models 3 and 5 are smaller than that obtained for the other models. Therefore, the models 3 and 5 are attained to resist the seismic loads. The

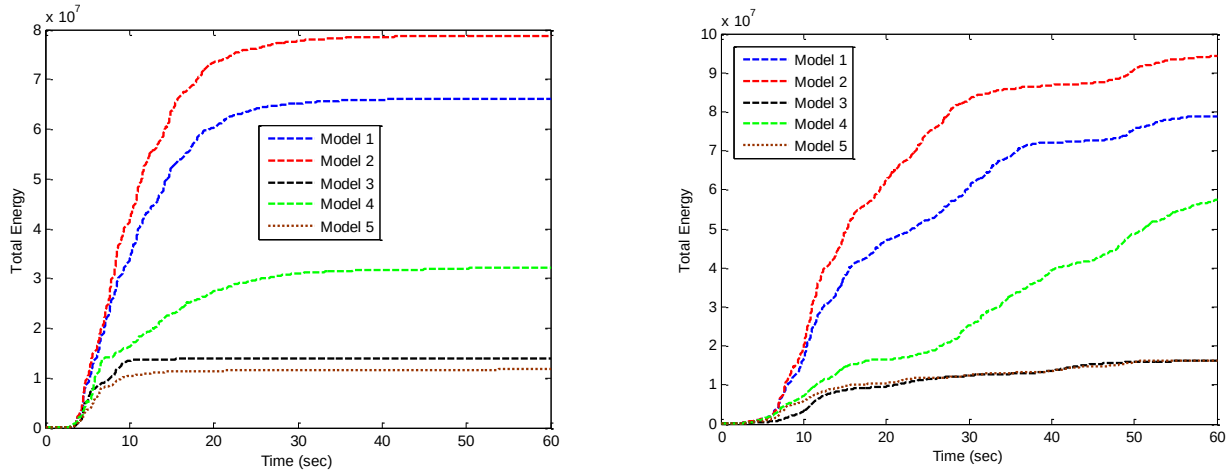

Fig. 9 Total energy of five models under (a) LA28 and (b) SE28

best model performance under LA28 is model 5 and the worst is model 2. Similarly, the models 3 and 5 performances are achieved under seismic SE28, while the performance of model 3 is seen better than model 5. Also, it can be shown that the performance of model 2 is the worst. Furthermore, the total energy performances of models illustrate the effect of seismic properties on the energy values.

In addition, the energy density of signals power is calculated under LA28 and SE28 and presented in Figure 10. And the linear fitting parameters of the energy density of the models are presented in Table 7, where energy density=a*(time)+b; here, a and b are the linear fitting parameters. The smallest parameters indicate the performance of the model should be a low probability of failure under seismic loads. The maximum density of models 1,2,3,4, and 5 are 2.67e+5, 3.13e+5, 1.73e+5, 2.15e+5, and 1.02e+5, respectively under LA28 seismic loads. And, the maximum density of models 1,2,3,4, and 5 are 2.37e+5, 3.38e+5, 7.32e+4, 9.97e+4, and 8.51+4, respectively, under SE28 seismic loads. Furthermore, the maximum density is occurred at times 4.64, 4.56, 4.5, 5.76, and 6.5 sec with models 1,2,3,4, and 5, respectively, under LA28; whereas the times of maximum densities of models 1,2,3,4, and 5 are 10.78, 10.96, 10.64, 28.86, and 7.06 sec, respectively for the SE28 seismic loads. Moreover, the period of wavelet density to release is 21.14, 23.20, 5.98, 23.82, and 5.14 sec for models 1,2,3,4 and 5, respectively, under LA28 and 49.14, 46.4, 10.56, 54.5, and 11.92 sec under SE28 loads, respectively. In addition, the evaluation of linear fitting shows that the lowest parameters are observed at models 3 and 5 under both seismic loads, and models 3 and 5 are also shown the best performance under seismic SE28 and LA28, respectively. Consequently, it can be concluded that the models 3 and 5 accomplish to decrease the signals power energy and density, while model 4 performances under LA28 and SE28 is shown worse in term of absorption of motion effect.

From these results, it is clear that the wavelet energy and density are able to estimate the performance of five frames, but we cannot distinguish between the performance of models 3 and 5; which model is the better and which is the worse. The above results reveal that the two models, 3 and 5 are better than other models. The performance of model 5 is seen well under LA28 load, whereas the performance of model 3 is shown best under seismic load SE28. Herein, it should be mentioned that the characteristics of ground motions may affect the performance of wavelet energy calculations.

To calculate the wavelet variance, the reconstructed signals are used to calculate CWT. Figure 11 demonstrates the variance components of models under four seismic loads. The time series of variance is presented in the figure. Here, the maximum variance of 1,2,3, 4 and 5 models' performances with LA14 are 9.87e+6, 1.01e+7, 1.07e+6, 1.23e+7, and 2.98e+6 mm2, respectively. In addition, the variance is released within 31.7 sec for models 1, 2 and 4; while it takes 17.86 sec with models 3 and 5. Furthermore, the performance of five models are seen similar under LA28, the maximum wavelet variance is shown high and low with models 4 and 3, respectively, while the five models take the same time to release the load effect. This indicates that the performance of models 3 and 5 are good to reduce the wavelet variance with time, but model 3 is better under LA ground motion effect. Similarly, the performance of five models has no changes under the seismic load SE04 and SE28. For SE04, the maximum variance of models 1, 2, 3, 4 and 5 are 2.62e+7, 1.68e+7, 9.28e+5, 2.64e+7, and 1.24e+6 mm2, respectively. The maximum wavelet variance of models 1,2,3,4 and 5 are 4.27e+7, 4.57e+7, 4.39e+6, 1.87e+7, and 1.17e+7 mm2, respectively. Furthermore, models 1, 2, and 4 take 44.48 sec to release the load affect under SE04 ground motion, while models 3 and 4 take 23 sec only. Releasing time is 56.32 sec for models 1 and 2, and 17.26 sec for models 3 and 5; while the response of model 4 is seen affected and obvious movement is seen after seismic load affect. These results reveal that the performance of mode 4 is worse under four seismic loads. In addition, the performance of model 3 outweighs the performance of model 5 under different

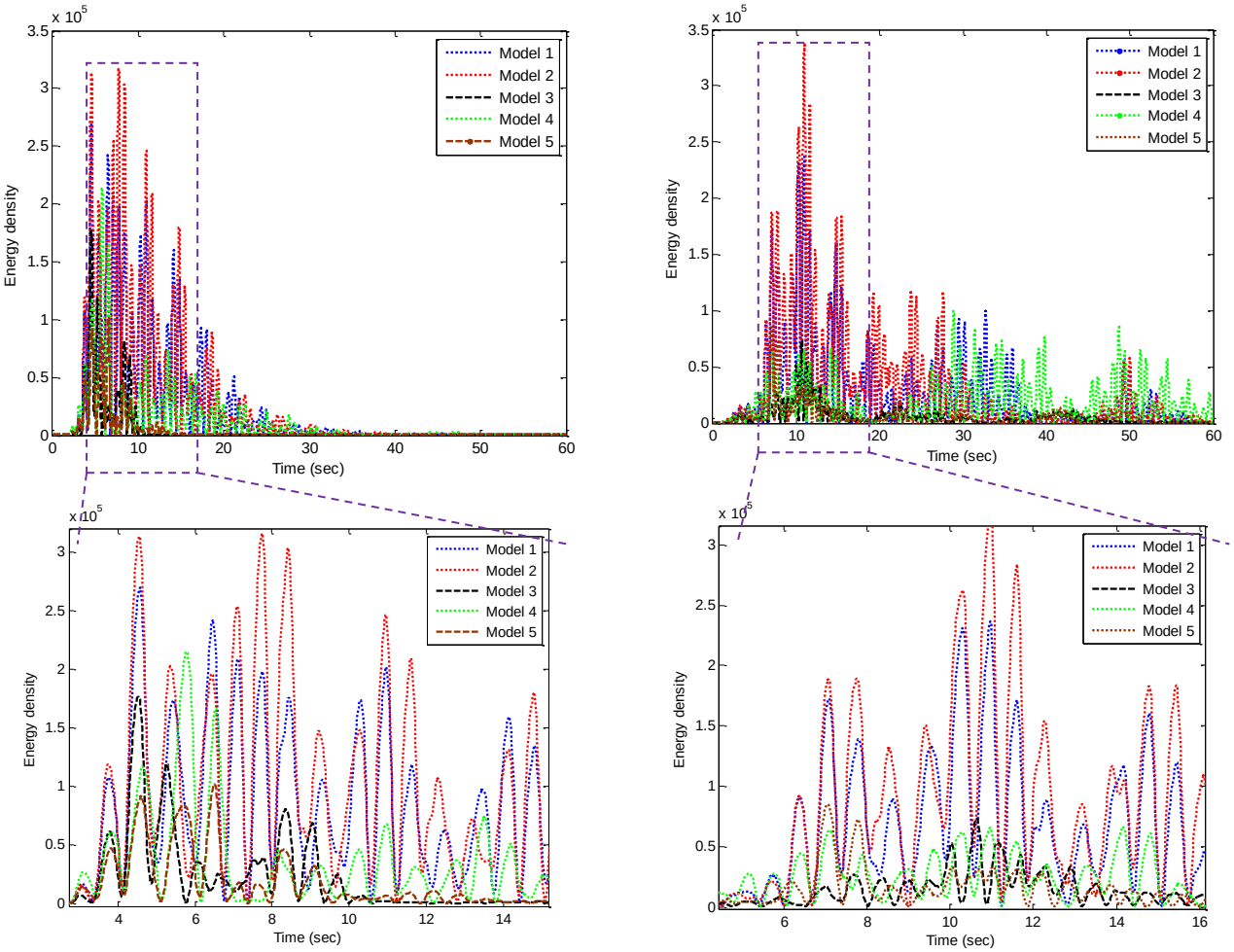

(a) (b)

Fig. 10 Energy density of five models under (a) LA28 and (b) SE28

Table 7 Linear fitting parameters of models' energy densities

Model	LA28		SE28	
	a (e^{+2})	b (e^{+4})	a (e^{+2})	b (e^{+4})
1	-14.0	6.4	- 8.3	5.1
2	-17.0	7.6	- 12.0	6.8
3	-3.7	1.6	- 1.7	1.1
4	-6.4	3.0	0.92	1.6
5	-3.0	1.3	- 2.0	1.1

ground motions. In addition, the wavelet variance has not affected by the ground motions' characteristics. Thus, the performance of model 3 is better than other models in two factors variance and release effective in the time.

In summary, the results that presented in Min (2017) concluded that the models 3 and 5 performance are better than other models performances based on traditional measurements analyses. He summarized the behavior of five models in the time domain using the behavior of each story of the building; roof displacements, dominant frequency, and base shear evaluations under forty ground motions. His study considered forty ground motions to estimate the best model. The results of this study conclude that the behavior of model 3 is better than other models in wavelet power and variance with considering these influences on the measurement time under four ground motions only. Wavelet energy and density can be used to estimate the better model based on cumulative wavelet energy and absorption motion affect using wavelet density. The wavelet variance can be used to estimate the performance and effect of models along the monitoring time under different ground motions properties. Therefore, the wavelet variance is a reliable tool that can be used to assess the behavior of structures under seismic loads.

4. Conclusions

This study investigates to use the wavelet variance and energy of roof displacement of nine-story CFS with five damage mitigation systems as a novel evaluation system for control systems of structures in the frequency domain. These models, basic (Model 1), reinforced (Model 2), bracing (Model 3), lead rubber bearing (LRB) (Model 4), and composite (Model 5) moment frames are evaluated and assessed under four ground motion effects. The Lose

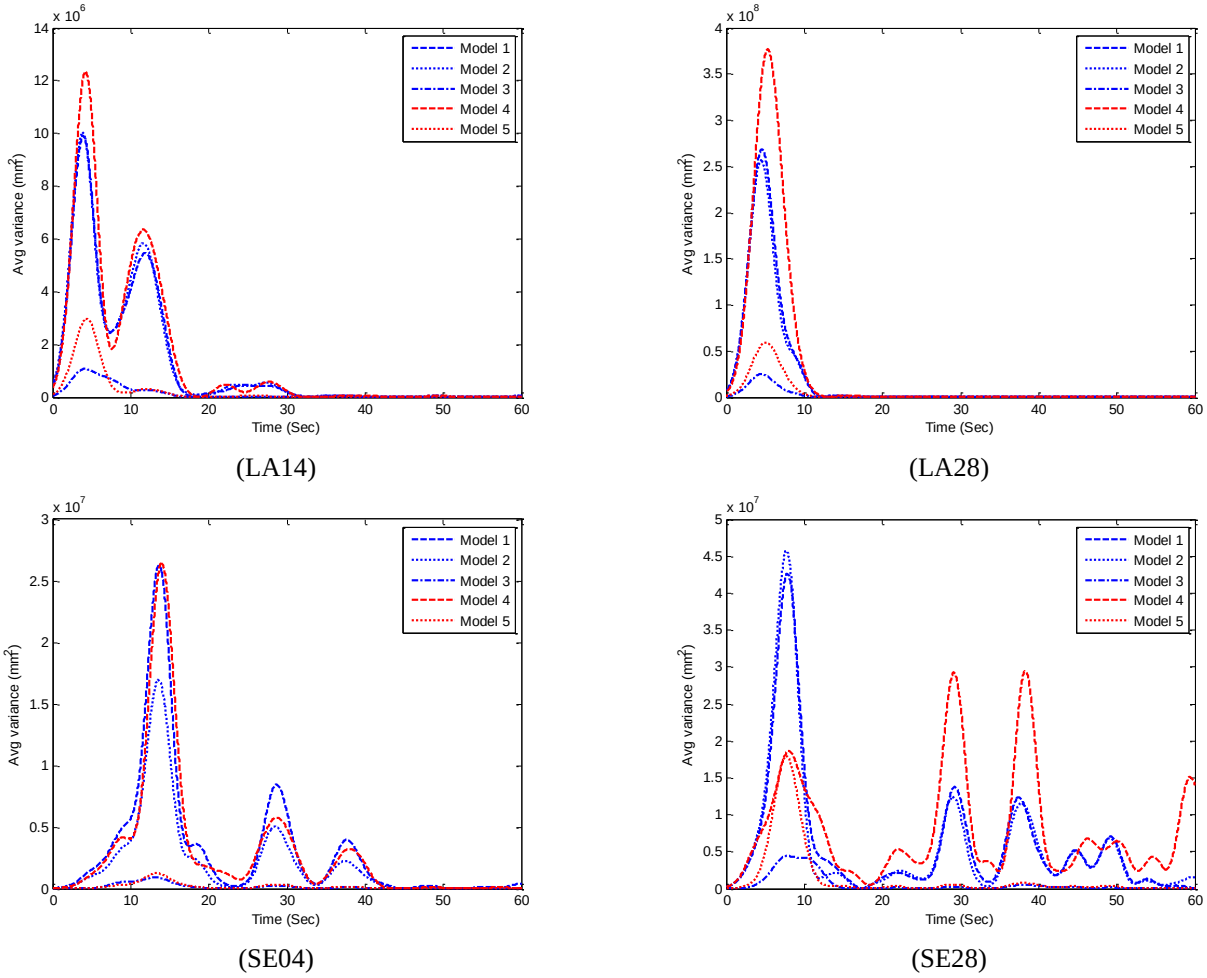

Fig. 11 Wavelet Variance of models under seismic' motions

Angeles (LA14 and LA28) and Seattle (SE04 and SE28) ground motions have been selected and used in the current study. The OpenSEES finite element models are designed and used to extract the model's behaviors. The discrete wavelet transforms (DWT) and continuous wavelet transform (CWT) are used and integrated to extract the wavelet energy and wavelet variance, respectively. The following conclusions are obtained:

The evaluation of displacement measurements of five models and conclusion of Min (2017) results show that the minimum amplitude is observed at models 3 and 5 under forty ground motions of LA and SE earthquakes. In addition, the maximum frequency is observed in model 3. These indicate that the performance of model 3 is more stability in the frequency domain. In addition, the behavior of model 5 is better than other models in the time domain.

The DWT can be used to extract the real behavior of structures, the detail wavelet component reflects the dynamic frames' behaviors. The detail components of wavelet levels of models 3 and 5 under loads of ground motions LA14 and SE04 show that the de-noise signals can be extracted using the wavelet analysis. The wavelet decomposition shows that the displacement response of models 3 and 5 are decreased higher than other models. The evaluation of wavelet energy for the five models under seismic LA28 and SE28 show that the models 3 and 5 behaviors are lower than other models, while the performance of model 3 is better than model 5 under SE28 ground motion. Moreover, the wavelet density evaluation illustrates that the performance of model 5 is better under LA28, whereas the performance of model 3 is best under seismic load SE28. The reconstruction signals are used to calculate the wavelet variance using CWT; and the results show that the behavior of model 3 is clearly better than that for other models in wavelet variance over the measurement time under different seismic loads. Therefore, the wavelet variance is a reliable tool that can be used to assess the behavior of structures under seismic loads.

Acknowledgments

This work was supported by the Incheon National University Institute of Convergence Science & Technology Research Grant in 2018.

References

Chan, Y. T. (1995), "Wavelet Basics", *Transform*, **99**(2), Springer, Germany. 1–26.

Chen, X. and Gao, Z. (2011), "Data Processing Based on Wavelet Analysis in Structure Health Monitoring System", *J. Comput.*, **6**(12), 2686–2691. https://doi.org/10.4304/jcp.6.12.2686-2691.

Chouinard, L., Shahsavari, V. and Bastien, J (2019), "Reliability of Wavelet Analysis of Mode Shapes for the Early Detection of Damage in Beams", *Front. Built Environ.,* **5,** 91. https://doi.org/10.3389/fbuil.2019.00091.

Farrokhi, H., Danesh, F. and Eshghi, S. (2010), "The structural detailing effect on seismic behavior of steel moment resisting connections", *Struct. Eng. Mech.*, **35**(5), 617-630. https://doi.org/10.12989/sem.2010.35.5.617.

Farzampour, A., Kamali-Asl, A. and Hu, J.W. (2018a), "Unsupervised identification of arbitrarily-damped structures using time-scale independent component analysis: Part I", *J. Mech. Sci. Technol.*, **32**(2), 567-577. https://doi.org/10.1007/s12206-018-0104-6.

Farzampour, A., Kamali-Asl, A. and Hu, J.W. (2018b), "Unsupervised identification of arbitrarily-damped structures using time-scale independent component analysis: Part II", *J. Mech. Sci. Technol.*, **32**(9), 4413-4422. https://doi.org/10.1007/s12206-018-0104-6.

Hu, J., Kang, Y., Choi, D. and Park, T. (2010), "Seismic Design, Performance, and Behavior of Composite-Moment Frames with Steel Beam-to-Concrete Filled Tube Column Connections", *J. Steel Struct.*, **10**(2), 177–191. https://doi.org/10.1007/BF03215829.

Hu, J. and Choi, E. (2014), "Seismic Design, Nonlinear Analysis, and Performance Evaluation of Recentering Buckling-restrained Braced Frames (BRBFs)", *J. Steel Struct.,* **14**(4), 683–695. https://doi.org/10.1007/s13296-014-1201-3.

Hu, J. and Roberto, L. (2011), "Analyses and evaluations for composite-moment frames with SMA PR-CFT connections", *Nonlinear Dyn*., **65**, 433–455. https://doi.org/10.1007/s11071-010-9903-3.

Hu, J. W. (2008), "Seismic Performance Evaluations and Analyses for Composite Moment Frames with Smart SMA PR-CFT Connections", Ph.D. Dissertation, Georgia Institute of Technology, U.S.A. http://hdl.handle.net/1853/22655.

Hu, J. W. (2015), "Seismic analysis and evaluation of several recentering braced frame structures", *J. Mech. Eng. Sci.*, **228**(5), 781–798. https://doi.org/10.1177%2F0954406213490600.

Iliuk, Itamar, José M. Balthazar, Angelo M. Tusset, Vinicius Piccirillo, Reyolando MLRF Brasil, and José RC Piqueira (2014), "The Use of Wavelets Analysis to Characterize the Dynamic Behavior of Energy Transfer vibrational systems", *Proceedings of the ASME 2014 International Design Engineering Technical Conferences & Computers and Information in Engineering Conference IDETC/CIE 2014*, DETC2014-34266. https://doi.org/10.1115/DETC2014-34266.

Jemai, S., Ellouze, M. and Abida, H. (2017), "Variability of Precipitation in Arid Climates Using the Wavelet Approach: Case Study of Watershed of Gabes in South-East Tunisia", *Atmosphere*, **8**, 178. https://doi.org/10.3390/atmos8090178.

Li, S., Zhang, L., Tang, J., Ling, D., and Wang, P. (2018), "Damage Identification in Timber Structures Based on Wavelet Singular Spectrum Entropy", *Math. Problem Eng.*, **2018**, **(**Article-ID-4898903), 9.

Kaloop, M. R., Hu, J. W., Sayed, M. A. and Seong, J. (2016), "Structural Performance Assessment Based on Statistical and Wavelet Analysis of Acceleration Measurements of a Building during an Earthquake", *Shock Vib.*, **2016**. https://doi.org/10.1155/2016/8902727.

Kaloop, M. R. and Hu, J. W. (2016), "Damage Identification and Performance Assessment of Regular and Irregular Buildings Using Wavelet Transform Energy", *Advances in Materials Science and Engineering*, **2016**. https://doi.org/10.1155/2016/6027812.

Kijewski, T. and Kareem, A. (2003), "Wavelet Transforms for System Identification in Civil Engineering", *Comput. Aided Civil Infrastruct. Eng.*, **18**(5), 339–355. https://doi.org/10.1111/1467-8667.t01-1-00312.

Kim, D.-H. and Leon, R. T. (2007), "Seismic Performance of PR Frames in Mid-America Earthquake Region", *J. Structu. Eng.*, **133**(12), 1808–1820. https://doi.org/10.1061/(ASCE)0733-9445(2007)133:12(1808).

Lee, S., Noh, S. and Lee, D. (2018), "Evaluation of Progressive Collapse Resistance of Steel Moment Frames Designed with Different Connection Details Using Energy-Based Approximate Analysis", *Sustainability*, **10**, 3797. https://doi.org/10.3390/su10103797.

Mansouri, I., Hu, J. W., Shakeri, K., Shahbazi, S. and Nouri, B. (2017), "Assessment of Seismic Vulnerability of Steel and RC Moment Buildings Using HAZUS and Statistical Methodologies", *Discrete Dynam. Nature Society*, **2017**. https://doi.org/10.1155/2017/2698932.

Mansouri, I., Ghodrati Amiri, G., Hu, J. W., Khoshkalam, M., Soori, S. and Shahbazi, S. (2017), "Seismic Fragility Estimates of LRB Base Isolated Frames Using Performance-Based Design", *Shock Vib.*, **2017**, https://doi.org/10.1155/2017/5184790.

Mansouri, I., Soori, S., Amraie, H., Hu, J. and Shahbazi, S. (2018), "Performance based design optimum of CBFs using bee colony algorithm", *Steel Compos. Struct.*, **27**(5), 613-622. https://doi.org/10.12989/scs.2018.27.5.613.

Matarazzo, T. J., Kurata, M., Nishino, H. and Suzuki, A. (2018), "Postearthquake Strength Assessment of Steel Moment-Resisting Frame with Multiple Beam-Column Fractures Using Local Monitoring Data", *J. Struct. Eng.*, **144**(2). https://doi.org/10.1061/(ASCE)ST.1943-541X.0001967.

Mehanny, S. and Deierlein, G. (2000), "Assessing seismic performance of composite (RCS) and steel moment framed buildings", *Proceedings, 12th World Conference on Earthquake Engineering,* http://www.iitk.ac.in/nicee/wcee/article/0746.pdf.

Mehanny, S. S. F. and Deierlein, G. G. (2001), "Seismic damage and collapse assessment of composite moment frames", *J. Struct. Eng.*, **127**, 1045–1053. https://doi.org/10.1061/(ASCE)0733-9445(2001)127:9(1045).

Min, S. H. (2017) "Probabilistic Seismic Performance Evaluation of Composite Moment Frame Structures with Seismic Damage Mitigation Systems". Ph.D. Thesis, Incheon National University, South Korea.

Park, T., Hwang, W. S., Leon, R. T. and Hu, J. W. (2011) "Damage evaluation of composite-special moment frames with concrete-filled tube columns under strong seismic loads", *KSCE Journal of Civil Engineering*, **15**(8), 1381–1394. https://doi.org/10.1007/s12205-011-1225-6.

Rhee, J., Chang, D. and Hu, S. (2012) "Advanced Analysis of Connections to Concrete-Filled Steel Tube Columns using the 2005 AISC Specification", *J. Korean Soc. Adv. Compos. Struct.* , **3**(3), 9–21. https://doi.org/10.11004/kosacs.2012.3.3.009.

Rioul, O. and Vetterli, M. (1991), "Wavelets and Signal Processing", *IEEE Signal Processing Magazine*, **8**(4), 14-38, https://doi.org/10.1109/79.91217.

Sayed, M. A., Kaloop, M. R., Kim, E. and Kim, D. (2017), "Assessment of Acceleration Responses of a Railway Bridge using Wavelet Analysis", *KSCE Journal of Civil Engineering*, **21**(5), 1844–1853. https://doi.org/10.1007/s12205-016-1762-0.

Seo, J. and Hu, J. (2016) "Seismic Response and Performance Evaluation of Self-Centering LRB Isolators Installed on the CBF Building under NF Ground Motions", *Sustainability*, **8**(2), 109. https://doi.org/10.3390/su8020109.

Shallan, O., Maaly, H. and Hamdy, O. (2018), "A developed design optimization model for semi-rigid steel frames using teaching-learning-based optimization and genetic algorithms",

Struct. Eng. Mech., **66**(2), 173-183. https://doi.org/10.12989/sem.2018.66.2.173.

Shi, G., Yin, H. and Hu, F. (2018), "Experimental study on seismic behavior of full-scale fully prefabricated steel frame: Global response and composite action", *Eng. Struct.*, **169**, 256–275. https://doi.org/10.1016/j.engstruct.2018.05.052.

De Stefano, A., Matta, E. and Clemente, P. (2016), "Structural health monitoring of historical heritage in Italy: some relevant experiences", *J. Civil Struct. Health Monitoring*, **6**(1), 83–106. https://doi.org/10.1007/s13349-016-0154-y.

Sun, Z. (2002), "Structural damage assessment based on wavelet packet transform", *J. Struct. Eng.*, **128**, 1354.

Taha, M. M. R. (2006) "Wavelet Transform for Structural Health Monitoring: A Compendium of Uses and Features", *Struct. Health Monitoring*, **5**(3), 267–295. https://doi.org/10.1177/1475921706067741.

Torrence, C. and Compo, G. P. (1998), "A Practical Guide to Wavelet Analysis", *Bullet. American Meteorological Soc.*, **79**(1), 62–78.

Xiaoyan, M., Junquan, Y. and Linguang, X. (2000), "Signal reconstruction based on mean threshold wavelet packet de-noising", *WCC 2000 - ICSP 2000. 2000 5th International Conference on Signal Processing Proceedings. 16th World Computer Congress 2000*, https://doi.org/10.1109/ICOSP.2000.894515.

Xing, L., Huang, L., Chi, G., Yang, L., Li, C. and Hou, X (2018), "A Dynamic Study of a Karst Spring Based on Wavelet Analysis and the Mann-Kendall Trend Test", *Water,* **10**, 698. https://doi.org/10.3390/w10060698.

PL